P. gingivalis Infection Upregulates PD-L1 Expression on Dendritic Cells, Suppresses CD8+ T-cell Responses, and Aggravates Oral Cancer

Junling Ren[1], Xiao Han[1], Hannah Lohner[1], Rosalie G. Hoyle[2,3], Jiong Li[2,3], Shuang Liang[4], and Huizhi Wang[1,5]

ABSTRACT

Accumulating evidence shows that PD-L1 expression on dendritic cells (DC) is critical for cancer immunotherapy and that *Porphyromonas gingivalis* (Pg) colonization aggravates the progression of upper gastrointestinal cancers. However, the effects of Pg infection on PD-L1 expression on DCs and related immune consequences in the infection milieu of oral cancer remain unexplored. Here, we found that Pg infection robustly enhanced PD-L1 expression on DCs in a gingipain-dependent manner in cultured cell and systemic infection assays. Pg infection suppressed antigen-specific CD8+ T cells through upregulation of PD-L1 expression on ovalbumin (OVA)-pulsed DCs. This suppression was manifested by decreased IFNγ, perforin, granzyme B, and CD107a. Further analysis showed that Pg drastically reduced CD8+ T cells' ability to lyse OVA-pulsed target cells. Additionally, Pg infection increased the phosphorylation of Akt and STAT3, leading to a significant increase in PD-L1 expression. This was substantiated by using siRNA, overexpression plasmids, and pharmacologic inhibitors. Consistent with the *in vitro* observations, in a syngeneic mouse oral cancer model, Pg infection significantly enhanced PD-L1 expression on DCs from intratumoral tissues and cervical lymph nodes and exacerbated oral cancer progression, whereas a Pg lysine-specific, gingipain-defective mutant failed to do so. These influences of Pg were largely diminished when tumor cells were pretreated with antibiotics or a STAT3 inhibitor. Therefore, we demonstrated that Pg infection upregulates PD-L1 expression on DCs through Akt-STAT3 signaling, suppresses CD8+ T-cell cytotoxicity, and aggravates oral cancer growth, suggesting targeting Pg, and/or its mediated signaling, could be a therapeutic strategy to improve the efficacy of checkpoint blockade immunotherapy.

Introduction

Activated CD8+ T cells [cytotoxic T lymphocyte (CTL)] express a range of effector molecules to defend against pathogens and cancer cells (1). Major CTL activities are mediated either directly by synaptic exocytosis of cytotoxic granules containing perforin (Prf) and granzyme B (GrB) into the target, resulting in infected or cancer cell destruction, or indirectly through secretion of cytokines such as interferon (IFN)γ to promote tumoricidal activity (2). Adhesion/co-stimulatory molecules on CTLs play a critical role in the T-cell receptor (TCR)–mediated lysis of target cells by interacting with their cognate ligands. In this regard, programmed cell death protein 1 (PD-1), an inducible immunoglobulin expressed on activated T and B lymphocytes, plays a key role in controlling peripheral tolerance and lymphocyte activation and has two ligands, PD-L1 (B7-H1) and PD-L2 (B7-DC). The binding of PD-1 to its ligands results in the inhibition of T-cell proliferation and secretion of cytokines. Therefore, PD-1 and its coligand interaction act as a threshold in the modulation of adaptive immunity by restraining the cytotoxic activity of CD8+ T cells. Such immunoregulatory properties of PD-1/PD-L1 signaling have been targeted for the development of novel therapies in chronic infections and tumor progression (3, 4), which have achieved highly impressive successes during the last decade (3, 5).

In the tumor microenvironment, PD-L1 is widely expressed on tumor cells and various immune cells including dendritic cells (DC), macrophages, and myeloid-derived suppressor cells (MDSC; refs. 6, 7). The expression of PD-L1 on tumor cells (tumoral PD-L1) has been approved by the US Food and Drug Administration as a companion diagnostic indicator for PD-L1/PD-1 blockade therapy (8). However, almost half of patients positive for tumoral PD-L1 do not respond to PD-L1 blockade, whereas some patients with PD-L1–negative tumor cells respond well (9–11). Importantly, a growing body of studies has demonstrated that PD-L1 expressed by DCs (DC-PD-L1) is critical for the regulation of CTLs in the tumor microenvironment (12–15). A lack of PD-L1 on DCs drastically reduces the therapeutic effect of PD-L1 blockade immunotherapy in different tumor models (12–15). Additionally, recent studies show that PD-L1 expression by myeloid cells could serve as the sole predictor of immune responses (15, 16). These findings highlight the significance of DC-PD-L1 in the efficacy of immune-checkpoint blockade therapy (12–14) and suggest that the relative contributions of PD-L1 on different lineages of cells remain incompletely understood and that further investigations are needed to clarify the working model of how PD-L1/PD-1 signaling inhibits immune responses.

Porphyromonas gingivalis (P. gingivalis) is a gram-negative, pathogenic oral bacterium that is associated with multiple systemic inflammatory diseases, such as atherosclerosis, arthritis, and some cancers (17). Apart from lipopolysaccharide, fimbriae, and capsule,

[1]VCU Philips Institute for Oral Health Research, Department of Oral and Craniofacial Molecular Biology, Virginia Commonwealth University, Richmond, Virginia. [2]Institute for Structural Biology, Drug Discovery and Development, Virginia Commonwealth University, Richmond, Virginia. [3]VCU School of Pharmacy, Department of Medicinal Chemistry, Virginia Commonwealth University, Richmond, Virginia. [4]Department of Molecular Pathobiology, New York University College of Dentistry, New York, New York. [5]Massey Cancer Center, Virginia Commonwealth University, Richmond, Virginia.

J. Ren and X. Han contributed equally to this article.

Corresponding Author: Huizhi Wang, Department of Oral and Craniofacial Molecular Biology, Virginia Commonwealth University, 521 N. 11TH, Richmond, VA 23298. Phone: 804-628-6386; Fax: 804-828-0150; E-mail: wangh3@vcu.edu

P. gingivalis secretes a unique group of cysteine proteases called gingipains that cleave extracellular matrix components, cell receptors, and intracellular molecules, demonstrating the involvement of this bacterium in various host cell responses (17). Our and other previous studies have demonstrated that *P. gingivalis* infection promotes the growth and metastasis of different cancers, suppresses chemotherapy-induced apoptosis, and worsens the prognosis of cancer patients (18–21). Moreover, recent studies show that *P. gingivalis* infection promotes anti-inflammatory macrophage polarization and enhances PD-L1 expression by oral epithelial and cancer cells (22–24). Notably, *P. gingivalis* infection is also found to affect the activity and differentiation of various T-cell subsets (25, 26). Because DC-PD-L1 was recently demonstrated to be critical for the efficacy of checkpoint blockade immunotherapy (13–15), it would be of paramount importance to know whether *P. gingivalis* infection affects DC-PD-L1 expression and the molecular mechanisms involved, as well as the subsequent influences on $CD8^+$ T-cell cytotoxicity and oral cancer progression.

In this study, we demonstrated for the first time that *P. gingivalis* infection enhanced the expression of DC-PD-L1 in a gingipain-dependent manner, which downregulated $CD8^+$ T-cell cytotoxicity and exacerbated oral cancer progression in a syngeneic mouse model. Moreover, we found that this increased DC-PD-L1 expression arose through modulation of Akt–STAT3 signaling. Considering the newly identified critical role of DC-PD-L1 in various cancers and chronic infections, measuring and targeting *P. gingivalis* and its associated signaling pathways will advance the understanding of *P. gingivalis*–induced immunosuppression and provide insights into improvement of immune-checkpoint blockade therapy.

Materials and Methods

Cell lines

EL4 T-lymphoma cells (EL4; ATCC TIB-39) were purchased from ATCC in 2022, and murine oral cancer cells (MOC1) were purchased from Kerafast in 2020. Both cell lines were authenticated using short tandem repeat profiling according to the vendor's information and not reauthenticated after acquisition. All cells were used at 1 to 5 passages after thawing and routinely tested for *Mycoplasma* contamination using the MycoAlert Mycoplasma Detection kit (Lonza, cat.# LT07-318) before each experiment. Both cell lines were expanded and frozen at early aliquots, and each were cultured for less than a total cumulative time of 6 months from the time of acquisition to the experiment. All cells (including DCs and T cells below) were cultured in 37°C, 5% CO_2 in RPMI-1640 medium (ThermoFisher, cat. #21870092) supplemented with 10% fetal bovine serum (R&D Systems, cat. #S11550H), 2 mmol/L L-glutamine (ThermoFisher, cat. #25030081), 20 mmol/L pH7.3 HEPES (Corning, cat. #25–060-CI), 7.5% (W/V) sodium bicarbonate (Corning, cat. #25-035-CI), 100 mmol/L sodium pyruvate (Corning, cat. #25-000-CI), 50 μmol/L 2-mercaptoethanol (Sigma, cat. #M3148-100ML), 1% penicillin/streptomycin (ThermoFisher, cat. #15140-122) and 2.5 mg/mL Plasmocin Prophylactic (InvivoGen, cat. #Ant-mpp).

Mice, bacteria, and cell culture

Ten- to 12-week-old C57/BL6 wild-type and C57BL/6-Tg (TcraTcrb)/J (also known as OT-I mice) female mice were obtained from the Jackson Laboratory. Mice were housed in the animal facility of Virginia Commonwealth University in accordance with animal care standards of the institution. Animal experiments were approved by Virginia Commonwealth University.

Different *P. gingivalis* strains including ATCC 33277, W83, and their isogenic mutants lacking lysine- or arginine-specific gingipain protease, described as ΔKgp and ΔRgp, respectively, were from Jan Potempa's Lab (University of Louisville School of Dentistry, Louisville, KY). The deletion of target genes was confirmed with PCR before use. The bacteria were cultured anaerobically in trypticase soy broth (BD Bacto; cat. #211825) supplemented with yeast extract (1 mg/mL, BD Bacto, cat. #212750), hemin (5 μg/mL, MilliporeSigma, cat. #51820), and menadione (1 μg/mL, MilliporeSigma, M9429). *Streptococcus sanguinis* SK36 (from Dr. Kitten's lab, Virginia Commonwealth University School of Dentistry) was grown at 37°C in Anoxomat jars (Spiral Biotech) under microaerobic conditions (7% H_2, 7% CO_2, 80% N_2, and 6% O_2) in brain heart infusion (BHI; Bacto) broth. Fms-related tyrosine kinase 3 ligand (Flt3l)- and granulocyte-macrophage colony-stimulating factor (GM-CSF)–mediated bone marrow–derived DCs, abbreviated as Flt3l-DCs and GMDCs, respectively, were generated according to the procedures described in previous studies (27, 28).

$CD3^+$ T cells were isolated from the spleens of wild-type and OT-I mice using a $CD3^+$ T-cell isolation kit (R&D System). DCs were infected with *P. gingivalis* or ΔKgp for 4 hours at MOI 10 for all *in vitro* cell infections. For bacterial treatment, DCs were directly seeded in either a 96- or 6-well plate for the indicated studies. All DCs and EL4 T-lymphoma cells (EL4) were cultured in RPMI-1640 medium and maintained at a temperature of 37∘C in a humidified growth chamber under 5% CO_2 as described above.

ELISA

For ELISAs in mixed lymphocyte reactions, 2×10^3 cells were plated into each well per 96-well U-shaped bottom microplate (ThermoFisher, cat. #168136) in RPMI-1640 medium as specified above. After coculturing for 3 days, cell-free supernatants were collected, and the production of IL2 and GrB was assayed using ELISA kits (ELISA MAX Mouse IL2 kit, cat. #431001, BioLegend; GrB Mouse ELISA kit, cat. #BMS6029, ThermoFisher) according to the manufacturer's instructions. 20 μL cell-free supernatants was first diluted 1:10 for IL2 assay and 100 μL was diluted 1:2 for GrB assay, followed by a serial 2-fold dilution until the dilution reached 1:80 and 1:16, respectively. Dilution buffer (including in the kit) and the supernatant from unstimulated cells were used as a blank and sham control, respectively. The recombinant standard proteins were included in the kit and a standard curve was generated in each assay. SpectraMax iD3 (Molecular Devices) was used for optical density (OD) measurements at 450 and 540 nm, in triplicate. The optical imperfections in the plate were corrected by subtracting OD at 540 nm from that at 450 nm. Concentrations were calculated using GraphPad Prism with the interpolation of a linear standard curve. The average of triplicate samples was used for quantification.

Western blots

For Western blots, DCs in 6-well plates were pretreated with type I IFN receptor 2 antibody (10 μg/mL, R&D Systems, cat. #AF1083), type II IFN antibody (0.5 μg/mL, R&D Systems, cat. #AF-585), isotype control (0.5 μg/mL, R&D Systems, cat. #AB-1098) antibody, Akti (2.5 μmol/L, SelleckChem, cat. #S7776), MK2206 (5 μmol/L, APEx-BIO, cat. #A3010), or WP-1066 (10 μmol/L, SelleckChem, cat. #S2796) for 2 hours, or transfected with specific *stat3* siRNA or a plasmid encoding *stat3* with a scramble siRNA and vehicle plasmid as controls for 72 hours (as described below), then challenged with *P. gingivalis* or ΔKgp for 0.5, 1, 2, 4, 6, 12, or 24 hours followed by lysis of cells with radioimmunoprecipitation assay (RIPA) buffer (MilliporeSigma, cat.

#R0278) containing ReadyShield Phosphatase and Protease inhibitor cocktail (MilliporeSigma, cat. #PPC2020). Protein concentrations were determined using the bicinchoninic acid (BCA) protein assay kit (ThermoFisher, cat. #23225). An equal amount of protein samples (10 μg) was separated in NuPage Novex 4% to 12% bis-Tris poly-acrylamide gels (Invitrogen, cat. #NP0326BOX) and electroblotted onto polyvinylidene difluoride membranes (PVDF; Millipore, cat. #03010040001). After blocking by 5% BSA (MilliporeSignma, cat. #A7906), PVDF membranes were incubated with primary antibodies at 4°C overnight and then secondary antibodies for 1 hour at room temperature. The primary antibodies used were: anti–PD-L1 (R&D Systems, #AF1019, 1:1,000), anti-phospho-Akt (Ser473; Cell Signaling Technology, #4058, 1:1,000), anti-phospho-STAT3 (Tyr705; Cell Signaling Technology, #9145, 1:1,000), anti-phospho-STAT3 (Ser727; Cell Signaling Technology, #9134, 1:1,000), anti-Akt (Cell Signaling Technology, #4691, 1:1,000), and anti-STAT3 (Cell Signaling Technology, #4904, 1:1,000). The secondary antibodies used were: HRP-linked anti-rabbit antibody (Cell Signaling Technology, #7074, 1:3,000) and HRP-linked anti-goat antibody (Santa Cruz, cat. #sc-2354, 1:3,000). Anti-β-actin (Cell Signaling Technology, #4970, 1:2,000), anti-GAPDH (Cell Signaling Technology, #5174, 1:2,000), and anti-P38 (Cell Signaling Technology, #9212, 1:2,000) were used as loading control antibodies for protein normalization. Images were acquired using the G:Box Chemi XXI (Syngene).

Stat3 siRNA and plasmid transfection

For transfections, 3×10^6 Flt3l-DCs were transfected with a library of four *stat3* siRNA with the following sequences: 5′ CUCAGAGG-GUCUCGGAAAU 3′, 5′ CCGCCAACAAAUUAAGA AA 3′, 5′ CUCAGAGGGUCUCGGAAAU 3′, 5′ GAGUUGAAUUAUCAG-CUUA 3′, 5′ CAGU UUACCACGAAAGUCA 3′. These siRNAs were arrayed as a SMARTPool (Dharmacon) and transfected using Lipofectamine RNAiMAX (ThermoFisher, cat. #13778075) according to the manufacturer's instructions. A scrambled siRNA was used as a control with the sequence: 5′ UUCUCCGAACGUGUCACGUdtdt 3′. The plasmid encoding STAT3 (Addgene, cat. #8706) and a vehicle control plasmid (Addgene, cat. #10792) were also transfected into DCs using Lipofectamine LTX/Plus reagent (ThermoFisher, cat. #15338100) following the manufacturer's procedure. After transfection for 72 hours, the cells were treated with *P. gingivalis* for 6 or 24 hours. The cells were lysed as described above for Western blots. Anti-STAT3 (Cell Signaling Technology, #4904, 1:1,000) and anti-GAPDH (Cell Signaling Technology, #5174, 1:2,000) were used to assess the transfection efficacy.

Lymphocyte isolation

Mice were euthanized by CO_2 asphyxiation followed by cervical dislocation and immersed in 75% ethanol for 3 to 5 minutes, then transferred to the biosafety cabinet. The spleen and cervical lymph nodes (CLN) were collected and placed in sterile 6-well plates (Corning Costar, cat. #07-200-83) with 3 mL 1× phosphate-buffered saline (PBS; ThermoFisher, cat. #10010) on ice. Spleen tissues were minced with a razor (ThermoFisher, cat. #G535010) and CLNs were dissociated with two frosted slides (ThermoFisher, cat. #12-548) followed by digestion with 1× PBS solution including 1 mg/mL collagenase A (Worthington, cat. #LS004174), 1 mg/mL DNase (MilliporeSigma, cat. #10104159001), and 2% heat-inactivated FBS (R&D Systems, cat. #S11550H) for 20 minutes at 37°C with 5% CO_2. The digested tissues were then passed through 70-mm cell strainers (MilliporeSigma, cat. #CLS431750) using mechanical force with the rubber end of a 5-mL syringe. Cell suspensions were then treated with

0.1M EDTA (ThermoFisher, cat. #15575) for 5 minutes at 37°C and washed 2 times with 1×PBS. After lysis of red blood cells with ammonium chloride potassium (ThermoFisher, cat. #A1049201), cells were collected by centrifugation at $450 \times g$ for 10 minutes at 4°C.

DCs and OT-I T-cell coculture

DCs were collected and seeded into U-bottom 96-well plates (ThermoFisher, cat. #168136) at 0.02×10^6 cells per well. Cells were treated with a serial concentration of ovalbumin (OVA) peptide 257–264 (SIINFEKL; 0.1, 0.5, 1, and 10 ng/mL, AnaSpec Inc., cat. #AS-60193) for 2 hours, followed by treatment with a STAT3 inhibitor, WP-1066 (10 μmol/L, SelleckChem, cat. #S2796) or PD-L1 antagonist binding peptide, (D)-PPA (NYSKPTDRQYHF; 5 mg/mL, R&D Systems) for 1 hour. The cells were then challenged with *P. gingivalis* or ΔKgp (MOI = 10) for 3 hours, followed by washing three times with 1× PBS (ThermoFisher, cat. #10010), and cocultured with 0.08×10^6 CD3$^+$ splenic T cells isolated from OT-I mice in RPMI-1640 medium as specified above. After coculturing for 3 days, cells were treated with 1:500 diluted eBioscience Protein Transport Inhibitor Cocktail (ThermoFisher, cat. #00-4980), which includes brefeldin A (5.3 mmol/L) and monensin (1 mmol/L), for 6 hours and then harvested for CD8$^+$ T-cell analysis of Prf, GrB, IFNγ, and CD107a, as well as PD-L1 on MHC-II$^+$CD11c$^+$PD-L1$^+$ cells by flow cytometry as described below. ELISAs (as described above) were also used as a confirmatory approach to examine the secretion of IL2 (ELISA MAX Mouse IL2, cat. #431001, BioLegend) and GrB (GrB Mouse ELISA, cat. #BMS6029, ThermoFisher). In addition, after challenge with *P. gingivalis* for 24 hours, the percentages of CD11b$^+$/CD11c$^+$, CD80$^+$/86$^+$, or CD3$^+$/CD8$^+$ cell populations were analyzed by flow cytometry as described below.

Cell staining and flow cytometry

Cocultured cells were blocked with a transport inhibitor cocktail as described above (ThermoFisher, cat. #00-4980) for 6 hours before harvest. They were then collected and washed twice with Flow Cyto-metry Staining Buffer (ThermoFisher, cat. #00-4505-51) and stained with Zombie Aqua (BioLegend, cat. #423101), to exclude dead cells, followed by incubation with CD16/CD32 antibody (ThermoFisher, cat. #14-0161-82) for 20 minutes on ice to block nonspecific Fc receptor binding. Cells were then incubated with the following fluorescently labeled anti-mouse antibodies from ThermoFisher: CD3-Alex700 (cat. #56-0032-82), CD8$^+$-APC-Cy7 (cat. #A18637), CD11c-PerCP-cy5.5 (cat. #45-0114-82), PD-L1–PE (cat. #12-5982-82), and CD107a-efluor450 (cat. #48-1071-82). The stained cells were then washed, fixed/permeabilized using eBioscience Fixation and Permeabilization Buffer Set (ThermoFisher, cat. #88-8824-00) and stained with PE-Cyanine 7-IFNγ (ThermoFisher, cat. #25-7311-82), APC-Prf (Thermo-Fisher, cat. #17-9392-80), and FITC-GrB (ThermoFisher, cat. #11-8898-82). Isotype control antibodies were also used including Rat IgG2b kappa (Alexa Fluor700, cat. #56-4031-80), Armenian Hamster IgG (PerCP/Cyanine5.5, cat. #45-4888-80), Rat IgG2a kappa (PE, cat. #12-4321-80), Rat IgG2a kappa (eFluor 450, cat. #48-4321-82), Rat IgG1 kappa (PE-Cyanine7, cat. #25-4301-82), Rat IgG2a kappa (APC, cat. #11-4321-81), and Rat IgG2a kappa (FITC, cat. #11-4321-80). Cells were acquired with an LSRFortessa flow cytometer (BD Biosciences). Data were analyzed with FlowJo v10 software (BD Biosciences).

Cross-presentation assay and CD8$^+$ T-cell cytotoxicity assay

The Flt3l-DCs (1×10^5/mL) were incubated with 1 ng/mL OVA (MP Biomedicals) for 2 hours, followed by challenge with *P. gingivalis* or ΔKgp (MOI = 10) for 3 hours. Cells were then washed three times

with warm PBS. Splenic CD8$^+$ T cells from OT-I mice were purified using a CD8$^+$ T-cell isolation kit (ThermoFisher, cat. #8804-6822-74) and primed via coculturing with DCs as above for 3 days. EL4 cells were used as target cells in cocultures with mouse CD8$^+$ cytotoxic T cells. Equal amounts of EL4 target cells, in two separated groups, were labelled with high and low concentrations of carboxy-fluorescein succinimidyl ester (CFSE; 1 and 0.1 μmol/L, eBioscience, cat. #65-0850-84), respectively. The 1 μmol/L-CFSE-labelled EL4 cells were prepulsed with OVA peptide (5 μmol/L, AnaSpec Inc., cat. #AS-60193) for 12 hours, mixed with 0.1 μmol/L-CFSE-labelled unpulsed cells (used as an internal control), and then cocultured with primed CD8$^+$ T cells at 5:1, 10:1, or 20:1 effector-to-target cell ratios in three independent replicates. After 6 hours of incubation, Zombie Aqua was used to assess cell viability, and living EL4 cells could then be monitored and analyzed using flow cytometry, showing negative staining with Zombie Aqua. Target cell killing (target cell lysis) by CD8$^+$ T cells was determined by calculating the number of low-concentration CFSE-stained cells minus the number of high-concentration CFSE-stained cells: $100\times$ [1 − (% of 1 μmol/L CFSE cells/% of 0.1 μmol/L CFSE cells)], as previously described (29).

Systemic bacterial infection assay

Ten- to 12-week-old C57/B6/J mice were randomly divided into four different groups for intraperitoneal (i.p.) injection of *P. gingivalis* 33277, *P. gingivalis* ΔKgp mutant, *S. sanguinis*, or PBS as a solvent control (1×10^8 bacterial cells in 100 μL PBS). Spleens were harvested 24 hours after i.p. injection. In a separate experiment, four groups of mice were orally infected with the same bacteria mentioned above every other day for three infection periods as described in our previous studies (23, 30). CLNs were collected after 30 days from the first infection. Splenocytes and lymphocytes were isolated as described above, then harvested and stained with antibodies to assess the expression of PD-L1 on MHC-II$^+$CD11c$^+$PD-L1$^+$ cells by flow cytometry as described above.

MOC1 cell inoculation induced syngeneic oral cancer model and IHC

MOC1 with/without pretreatment of *P. gingivalis* 33277 were inoculated into 10- to 12-week-old wild-type C57/BL6 mice ($n = 5$ to 7) tongues. Mice were then orally infected with 1×10^9 CFU of the bacteria above suspended in 100 μL of PBS with 2% carboxymethyl-cellulose (MilliporeSigma, cat. #C4888) for a total of three times every other day. Additional experimental groups included intraperitoneally administering WP-1066 (10 mg/kg) every other day or metronidazole (5 mg/mL) *ad libitum* in drinking water for 30 days with/without bacterial infection. Control groups included untreated mice or those treated with antibiotic water or inhibitor only. In a separate experiment, we also examined the effect of the ΔKgp mutant using the same protocol outlined above. Additionally, to examine the clinical relevance of *P. gingivalis* infection in tumor progression under the natural infection milieu of the oral cavity, we modified this model by orally infecting mice every other day for three infection periods, followed by inoculation with uninfected MOC1 cells. The mice were euthanized with CO$_2$ and cervical dislocation 24 days after the final infection on the sixth day. Tumor growth was evaluated after the mice were sacrificed via measuring the area of each tumor mass by three different operators, which was used to represent approximate tumor volume as described in a previous study (31). Given there is not a widely accepted measuring approach to estimate the tumor volume in a MOC1-mediated syngeneic model, we used an approach from the clinical practice guideline, Response Evaluation Criteria in Solid Tumors v.1.1.

(RECIST 1.1), in which the largest diameter of each tumor mass was measured to represent its volume (18, 32).

After tongue-bearing tumors were collected, tumors were cut in the middle along the longest direction, fixed in 4% paraformaldehyde, embedded in paraffin wax, and stained with hematoxylin and eosin (H&E) using a staining kit (Vector Laboratories, cat. #H-3502). Tissue blocks were prepared and cut into 4-μm sections, with the first three sections from each half block used to calculate the largest diameter of each tumor. Measurements were performed under microscopy after HE staining. Additionally, CLNs were harvested. Lymphocytes were isolated as described above, followed by the analysis of PD-L1 by flow cytometry. The paraffin-embedded tissue sections were also used for immunostaining with mouse CD11c (Bioss, cat. #bs-2508, dilution 1:100) and PD-L1 (ThermoFisher, cat. #14-5982-82, dilution 1:100) antibodies, followed by secondary goat-anti-rabbit Alexa Fluor 488–(ThermoFisher, cat. #A11034, dilution 1:1,000) or goat-anti-rat Alexa Fluor 647 (ThermoFisher, cat. #44181, dilution 1:1,000)-conjugated IgG. PBS containing normal goat serum (R&D Systems, AB-1908, dilution 1:1,000) was used as a sham control. Images were captured using a fluorescence microscope (Nikon Elipse E800) and processed by Neurolucida, an image analysis software designed by MBFBioscience that can accurately perform fluorescence signal analysis. Quantification of the percentage of the PD-L1–positive area in region of interest (ROI) was performed using the image processing software ImageJ (Fiji; https://imagej.net/Fiji/Downloads), following the standard recommended algorithm (33). The images were imported and processed with color deconvolution and adjusted by threshold and measurement settings to get the percentage of positive areas.

Statistical analyses

The statistical significance of differences between multiple groups was evaluated by the analysis of variance (ANOVA), one-way or two-way, followed by the Tukey multiple comparison test using the InStat program (GraphPad). A two-tailed unpaired Student *t* test was used for the comparison between the two groups. All described results are representative of at least three independent experiments. Statistical analyses and the number of samples (n) are described in detail in the legend for each figure panel. Data were presented as the mean $\pm$ standard error (SE). A value of $P < 0.05$ was considered statistically significant. *, **, ***, and ****, represent $P < 0.05$, $P < 0.01$, $P < 0.001$, and $P < 0.0001$, respectively. The experiments were not randomized, except that the mice were randomly grouped before treatment.

Data availability

The data generated in this study are available upon request from the corresponding author.

Results

P. gingivalis infection upregulates PD-L1 expression on DCs in a gingipain-dependent manner

PD-L1 is reported to be constitutively expressed on the surface of DCs to restrain the activation of effector T cells (34). Using 10 day-cultured GMDCs and Flt3l-DCs, we first examined if *P. gingivalis* infection affected the frequency and maturation of DCs. Compared with unstimulated controls, *P. gingivalis* infection elevated expression of CD80/CD86, but did not substantially change the expression of CD11b and CD11c on either kind of DCs (Supplementary Fig. S1), indicating *P. gingivalis* infection may affect DC maturation with little influence on the number of DCs. Next, we examined PD-L1 expression on GMDCs in response to *P. gingivalis* infection.
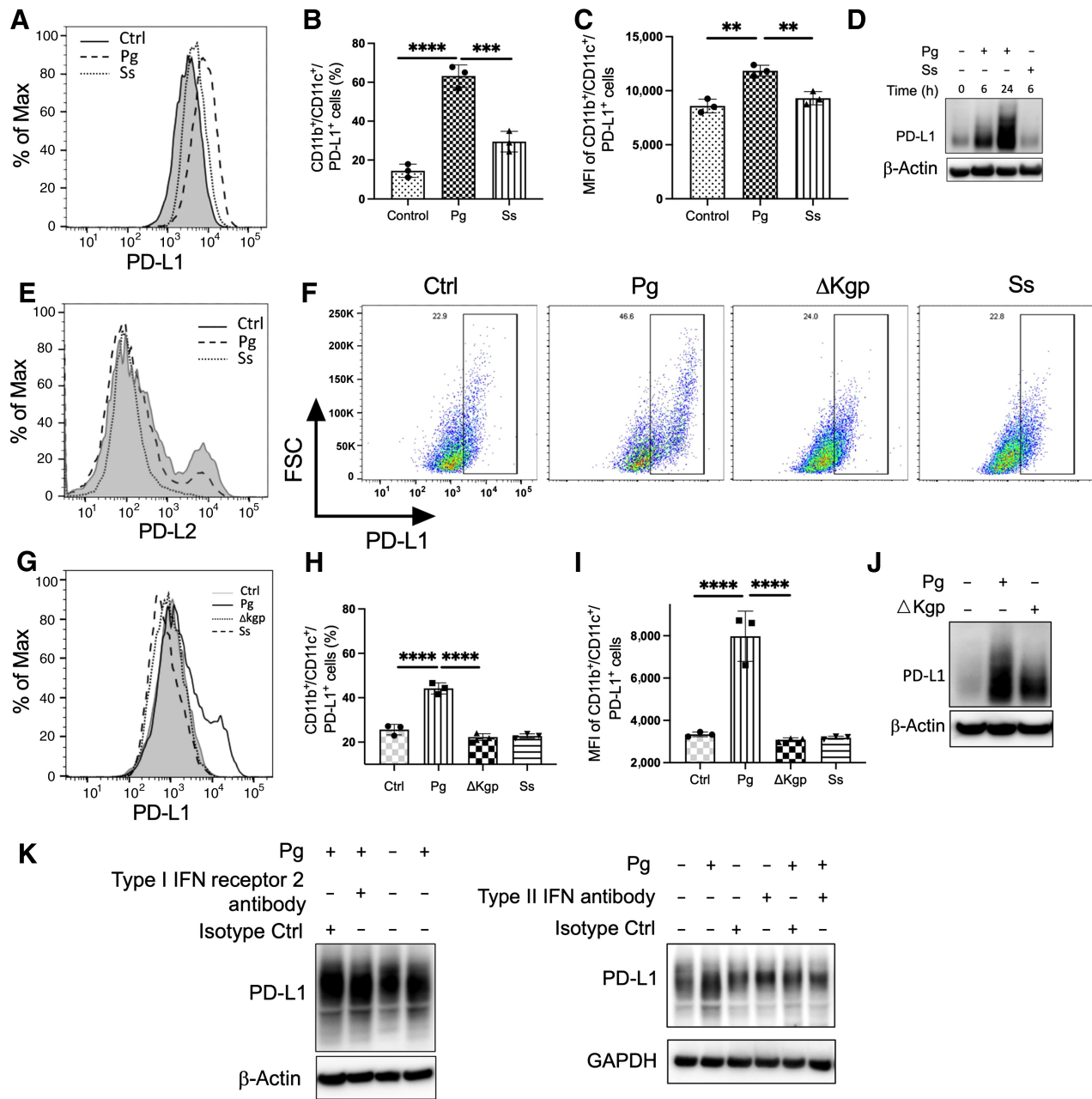
Figure 1.
P. gingivalis infection enhances the expression of PD-L1 on GMDCs and Flt3l-DCs in a gingipain-dependent manner. **A,** Representative flow cytometry histogram of PD-L1 on GMDCs upon *P. gingivalis* challenge. **B** and **C,** The percentage of GMDCs expressing PD-L1 and the mean fluorescence intensity (MFI) of PD-L1–positive GMDCs. **D,** Western blots showing PD-L1 expression after *P. gingivalis* infection. **E,** Representative flow cytometry histograms showing the expression of PD-L2 on GMDCs after *P. gingivalis* infection. **F** and **G,** Representative flow cytometry dot plots and histograms showing PD-L1 expression on Flt3l-DCs after *P. gingivalis*, ΔKgp mutant, and *S. sanguinis* infection. **H,** The percentage of Flt3l-DCs expressing CD11b/CD11c/PD-L1 and (**I**) the MFI of PD-L1–positive Flt3l-DCs. **J,** Western blots showing expression of PD-L1 in Flt3l-DCs after *P. gingivalis* and ΔKgp infection. **K,** Type I receptor 2 and type II interferon neutralization antibodies were used to pretreat Flt3l-DCs for 2 hours followed by *P. gingivalis* infection for 24 hours, and then cell lysates were harvested for subsequent Western blotting analysis for expression of PD-L1 on Flt3l-DCs. Left: neutralization antibody targeting type I interferon receptor 2. Right: neutralization antibody targeting type II interferon. Each symbol represents an experimental replicate and data are shown as mean ± SE. Results are representative of 3 independent experiments. Statistical significance was determined by one-way ANOVA with the Tukey multiple comparisons test. **, $P < 0.01$; ***, $P < 0.001$; ****, $P < 0.0001$.

We found that *P. gingivalis* infection significantly increased PD-L1 expression on GMDCs compared with the unstimulated or the commensal bacterium-, *S. sanguinis*, stimulated cells (**Fig. 1A–C**), which was further confirmed by Western blot (**Fig. 1D**). We did not observe any notable changes in PD-L2 expression on DCs (**Fig. 1E**). Because GM-CSF stimulation preferentially expands the type 2 conventional DC (cDC2) subset, whereas Flt3l stimulation expands higher percentages of type 1 cDCs (cDC1; ref. 35), we next examined if *P. gingivalis* infection promoted PD-L1 expression on Flt3l-DCs. The expression of PD-L1 on Flt3l-DCs robustly increased upon *P. gingivalis* challenge (**Fig. 1F–J**).

Given that Flt3l-mediated cDC1 cells are more efficient in tumor antigen cross-presentation compared with CD8^{+} T cells (36, 37), we used Flt3l-DCs throughout this study. To investigate the virulence factors of *P. gingivalis* in the regulation of PD-L1 expression, we next examined if infection with the ΔKgp mutant affected PD-L1 expression on Flt3-DCs. The absence of gingipain abrogated the ability of *P. gingivalis* to upregulate the expression of PD-L1 (**Fig. 1F–J**), which was further confirmed by Western blot (**Fig. 1J**). Because interferon is a dominant contributor to the expression of PD-L1 on DCs (38, 39), we also utilized neutralization antibodies to block type I IFN receptor 2 and type II interferon to examine if *P. gingivalis* promoted PD-L1
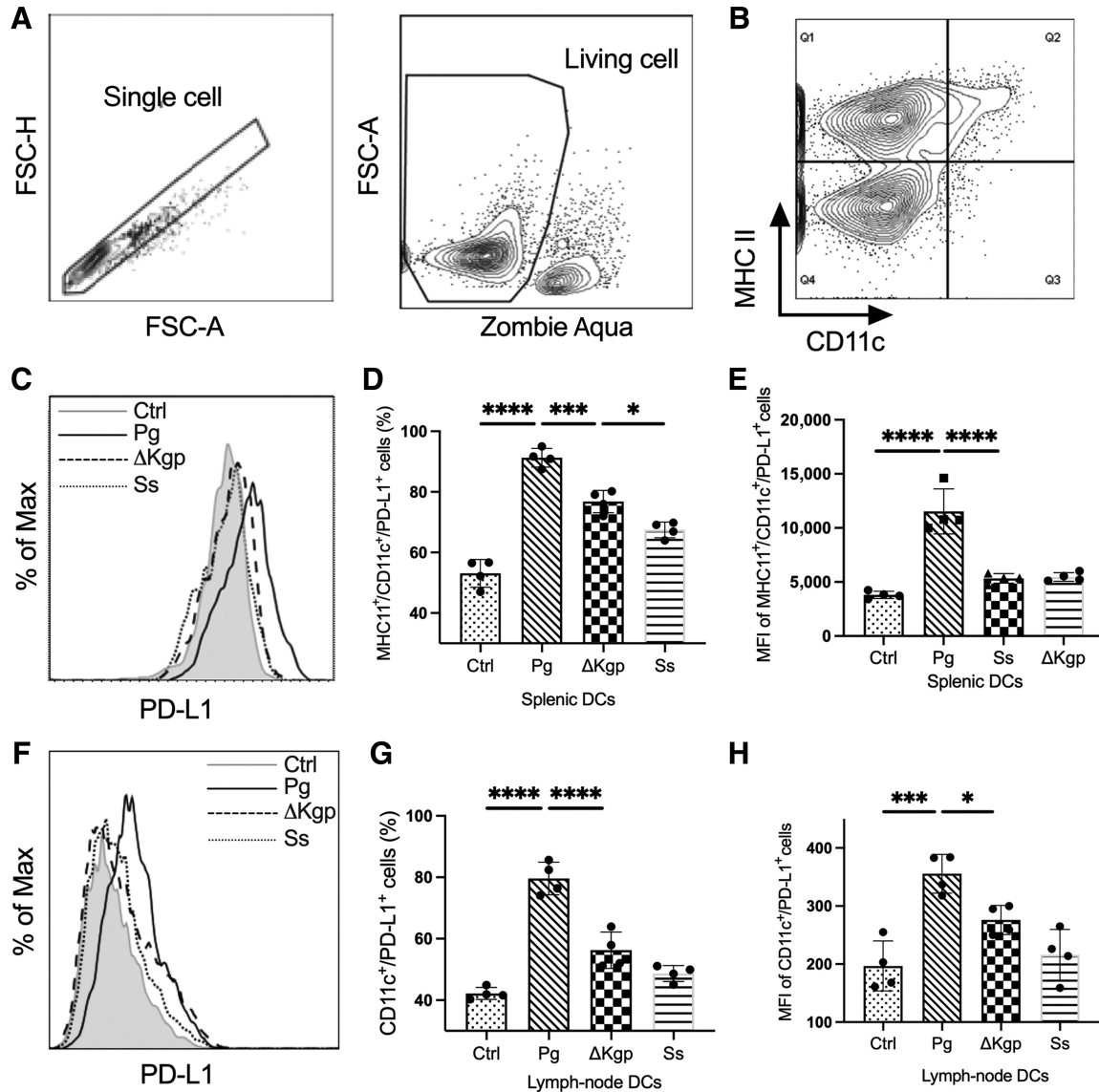

Figure 2.
P. gingivalis infection promotes the expression of PD-L1 on DCs *in vivo*. **A,** Density plots showing the gating strategy used to assess DC populations from mouse spleens via selecting MHC-II^{+} CD11c^{+} cells. **B,** Flow cytometry plots showing the purity of CD11c^{+}MHC-II^{+} cells. **C,** Representative flow cytometry histograms showing PD-L1 expression on splenic DCs. **D** and **E,** The percentages of splenic CD11c^{+}MHC-II^{+} cells expressing PD-L1 (**D**) and MFI of PD-L1–positive CD11c^{+}MHC-II^{+} cells (**E**). **F** and **G,** For orally infected mice, CLNs were collected 30 days after infection. Lymphocytes were harvested and stained with CD11c- and PD-L1–specific antibodies. Flow cytometry analysis showing CD11c^{+}PD-L1^{+} cells and PD-L1 expression after *P. gingivalis*, ΔKgp mutant, or control commensal bacterial infection. Each symbol represents an individual mouse, and data are shown as mean ± SE (*n* = 4 mice). Statistical analysis was performed using one-way ANOVA with the Tukey multiple comparisons test. Results are representative of 3 independent experiments. *, $P < 0.05$; ***, $P < 0.001$; ****, $P < 0.0001$.
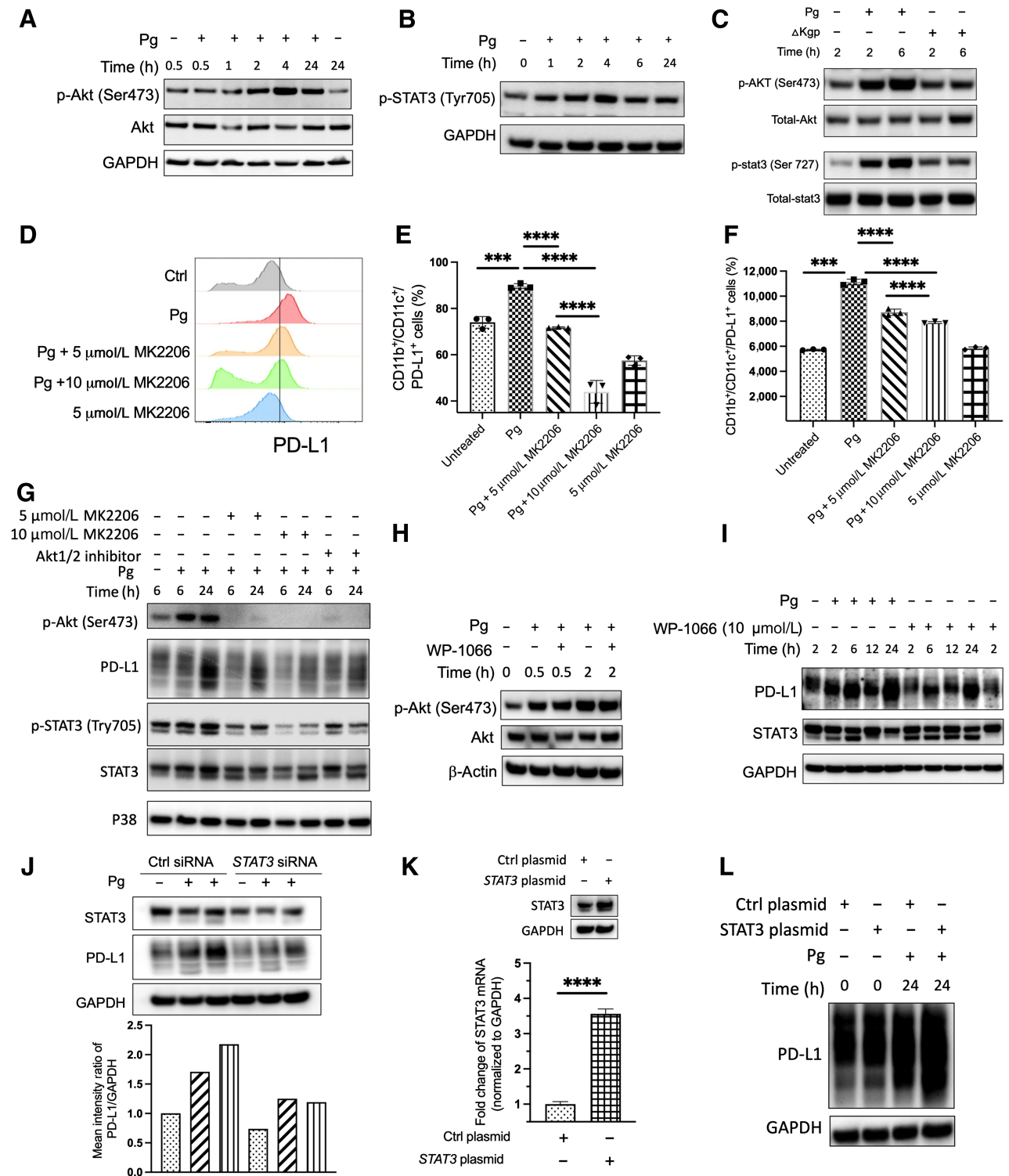
Figure 3.

P. gingivalis infection activates Akt–STAT3 signaling and thereby promotes the expression of PD-L1 on DCs. **A–C,** Western blots showing the dynamic phosphorylation of Akt and STAT3 in *P. gingivalis*– or ΔKgp-infected Flt3l-DCs. **D–F,** Flow cytometry analysis showing PD-L1 expression in *P. gingivalis*–challenged Flt3l-DCs with/without the Akt inhibitor MK2206. Each symbol represents an experimental replicate, and data are shown as mean ± SE. Statistical significance was determined by one-way ANOVA with Tukey multiple comparisons test. ***, $P < 0.001$; ****, $P < 0.0001$. **G–L,** Flt3l-DCs were pretreated with various Akt inhibitors, Akti (targeting Akt1/2), MK2206 (5 μmol/L), or WP-1066 (10 μmol/L) for 2 hours or transfected with specific *stat3* siRNA or a plasmid encoding *stat3* with a scramble siRNA and vehicle plasmid as controls.   (*Continued on the following page.*)
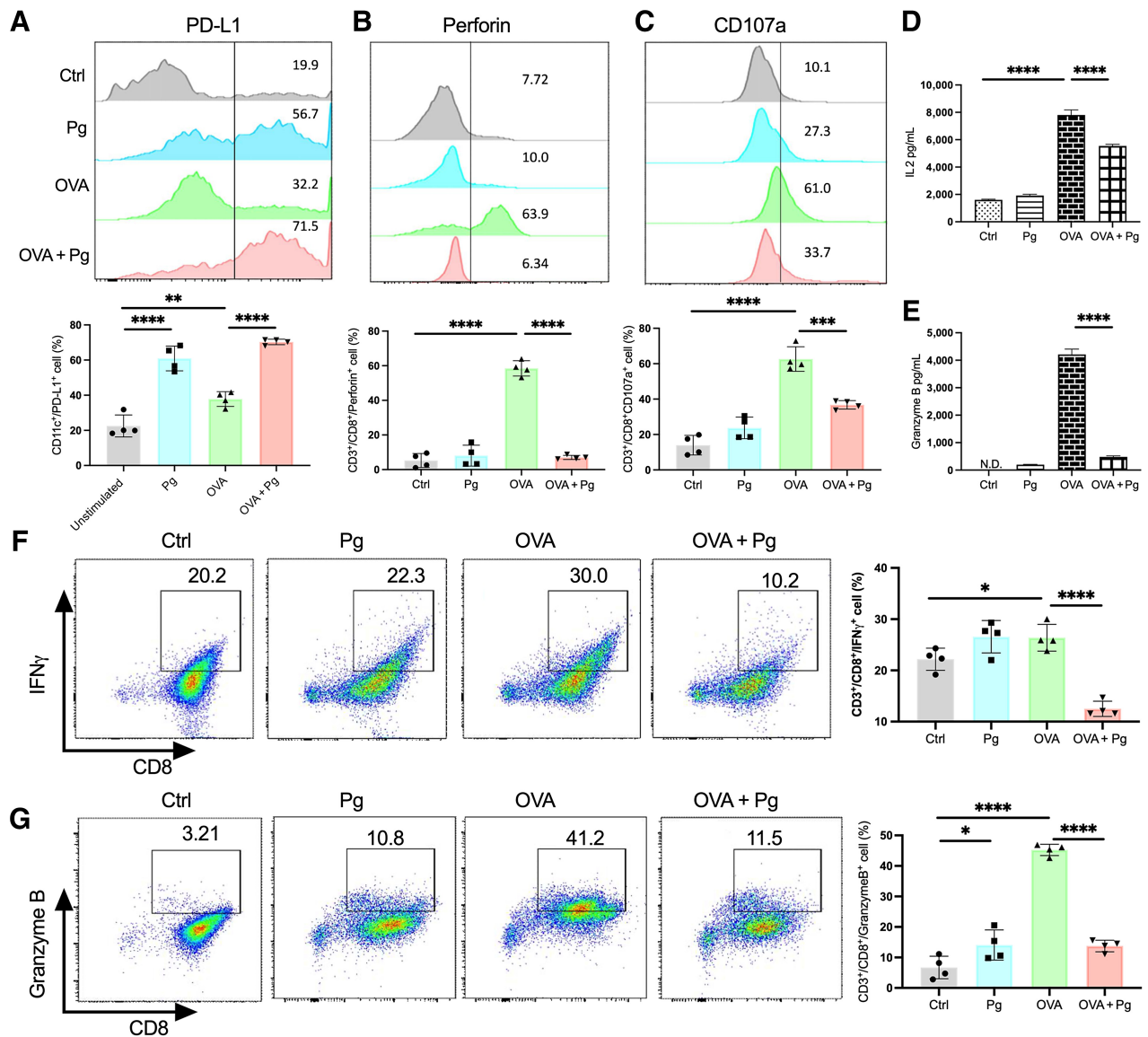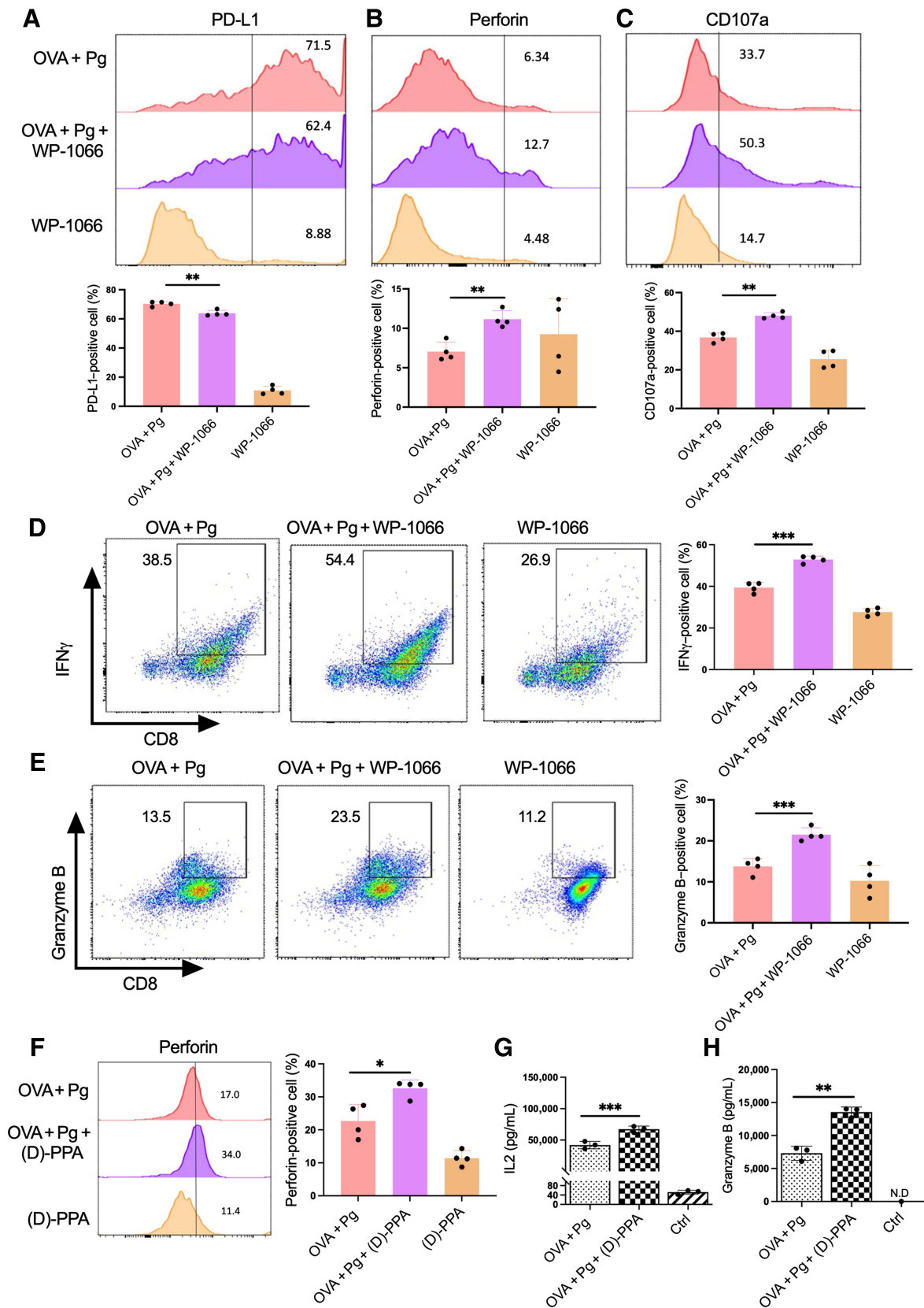
Figure 4.
P. gingivalis infection promotes DC-PD-L1 and suppresses CD8$^+$ T-cell activity. **A,** Flow cytometry histograms showing the expression of PD-L1 on CD11c$^+$ Flt3l-DCs with a pretreatment of *P. gingivalis*, OVA, or both for 3 hours and a subsequent coculture with OT-I CD8$^+$ T cells for 3 days. **B** and **C,** Representative plots showing Flt3l-DC–primed CD8$^+$ T cells expressing perforin (**B**) or CD107a (**C**). The bar figures in lower row showed the percentages of positive DCs (**A**) or CD8$^+$ T cells (**B** and **C**). **D** and **E,** Coculture supernatants were harvested, and the CD8$^+$ T-cell production of IL2 (**D**) and granzyme B (**E**) was assessed by ELISA. **F** and **G,** Flow cytometry showing percentages of Flt3l-DC–primed CD8$^+$ T cells expressing IFNγ (**F**) and granzyme B (**G**). Each symbol represents an experimental replicate, and data are shown as mean ± SE. Results are representative of 3 independent experiments. Statistical significance was determined by one-way ANOVA with Tukey multiple comparisons test. *, $P < 0.05$; ****, $P < 0.0001$.

expression through the *de novo* synthesis of interferons. No substantial changes of PD-L1 were observed on DCs between treatments with neutralization antibodies and isotype controls (**Fig. 1K**), indicating that interferon may not be involved in *P. gingivalis*–enhanced PD-L1 expression. Altogether, our results demonstrate that *P. gingivalis*

infection promotes PD-L1 expression on DCs, and the gingipain protease is a key factor in this process.

We next examined PD-L1 expression on splenic DCs (MHC-II$^+$ CD11c$^+$; **Fig. 2A** and **B**) from mice inoculated with *P. gingivalis* or its mutant, ΔKgp, for 24 hours. Likewise, *S. sanguinis* was used as

---

(*Continued.*) Western blotting was performed to assess PD-L1 expression and STAT3 phosphorylation after inhibition of Akt (**G**); phosphorylation of Akt in *P. gingivalis*–stimulated DCs after inhibition of STAT3 (**H**); and *P. gingivalis* induced DC-PD-L1 after WP-1066 and siRNA-mediated STAT3 inhibition (**I** and **J**) or overexpression of STAT3 in DCs (**K** and **L**). The transfection efficiency was estimated by the expression of total STAT3 (**J** and **K**). For the fold change of STAT3 mRNA, data represent three independent experiments. Error bars represent the mean ± SE. Statistical significance was determined by a two-tailed unpaired *t* test. ****, $P < 0.0001$. GAPDH or total P38 were probed as a loading control. All the blots and flow cytometry assays are representative of 3 independent experiments.
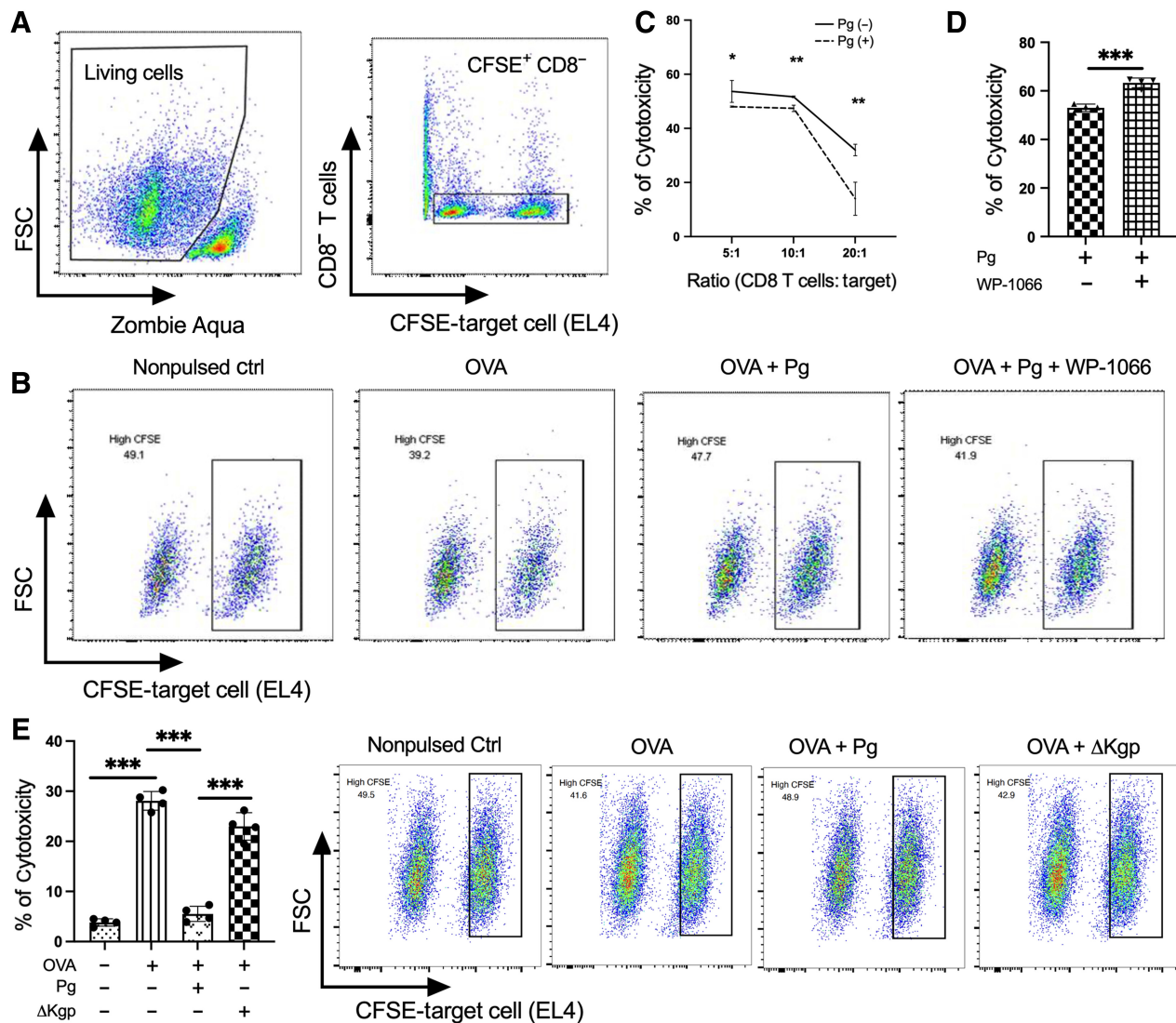
Figure 6.
P. gingivalis infection dampens the cytotoxicity of CD8^{+} T cells. **A,** Left: density plot and dot plots showing the gating strategy for the cytotoxicity assay using Zombie Aqua staining to assess cell viability. Right: distinct CFSE-labeled target EL4 cell population. **B,** Representative cytometry dot plots showing the cytotoxicity determined by the percentage of lysed EL4 cells after coincubation with activated OT-I CD8^{+} T cells for 6 hours. **C,** Quantification of the percentage of specific lysis, as described in Materials and Methods, in a cytotoxic assay with different effector/target cell ratios upon the challenge with *P. gingivalis* ($n = 5$ mice). Error bars represent the mean $\pm$ SE. Statistical significance was determined by two-way ANOVA with the Tukey multiple comparisons test. *, $P < 0.05$; **, $P < 0.01$. **D,** The percentage of lysed EL4 cells showing the effect of STAT3 inhibitor (WP-1066) on the cytotoxic activity of OT-I CD8^{+} T cells after 6 hours of coincubation. Each symbol represents an experimental replicate, and error bars represent the mean $\pm$ SE. Statistical significance was determined by a two-tailed unpaired *t* test. ***, $P < 0.001$. **E,** The percentage (left) and representative cytometry dot plots (right; $n = 4$ mice) of specific lysis of EL4 cells showing the different cytotoxic activity of CD8^{+} T cells after 3 days of coculturing with OVA-pulsed DCs with/without pretreatment of *P. gingivalis* or ΔKgp. Each symbol represents an experimental replicate, and data are shown as mean $\pm$ SE. Statistical significance was determined by one-way ANOVA with the Tukey multiple comparisons test. ***, $P < 0.001$. Results are representative of 3 independent experiments.

Figure 5.
P. gingivalis infection suppresses CD8^{+} T-cell activity through modulation of STAT3 activity. **A–E,** Flow cytometry showing the effect of STAT3 inhibitor (WP-1066) on the expression of PD-L1 on OVA-pulsed Flt3l-DCs, which were pretreated with *P. gingivalis* and/or STAT3 inhibitor for 3 hours and subsequently cocultured with OT-I CD8^{+} T cells for 3 days (**A**) and largely restored *P. gingivalis*–mediated decreases of Prf (**B**), CD107a (**C**), IFNγ (**D**), and GrB (**E**) secreted by Flt3l-DC–primed CD8^{+} T cells after 3 days of coculture. **F–H,** Flow cytometry and ELISA assays show that blockade of PD-L1 with (D)-PPA peptide significantly increased the percentage of perforin positive Flt3l-DC–primed CD8^{+} T cells (**F**), and the production of IL2 (**G**) and GrB (**H**) in supernatants after 3 days of coculture, as compared with controls. Each symbol represents an experimental replicate and data are shown as mean $\pm$ SE. Results are representative of 3 independent experiments. Statistical significance was determined by one-way ANOVA with the Tukey multiple comparisons test. *, $P < 0.05$; **, $P < 0.01$; ***, $P < 0.001$.
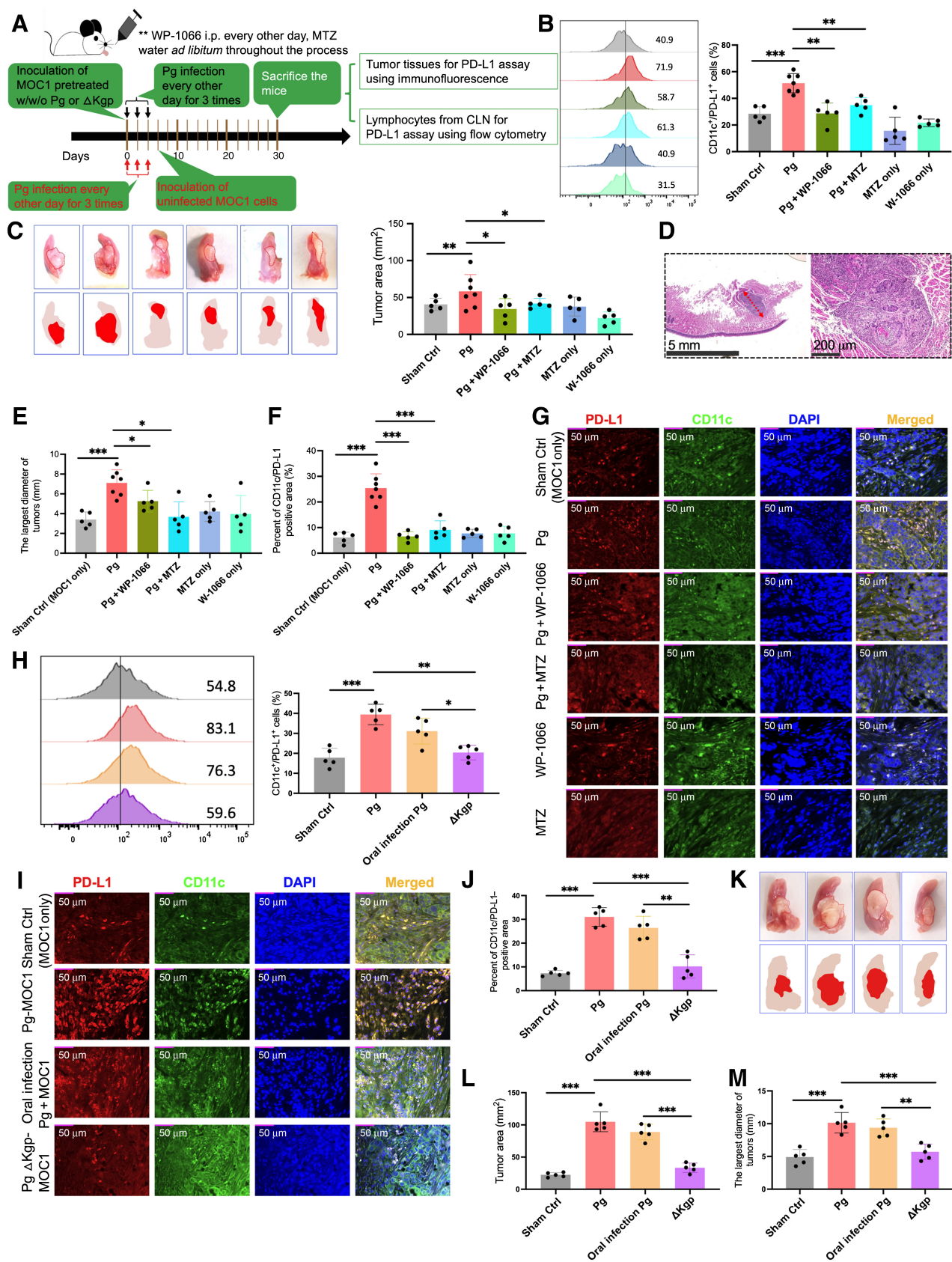
a commensal control bacterium. *P. gingivalis* significantly enhanced PD-L1 expression on CD11c⁺MHC-II⁺ cells, whereas ΔKgp largely lost this ability, compared with infection with the commensal bacterium (**Fig. 2C–E**). Additionally, we used an *in vivo P. gingivalis* chronic infection model, as performed in our previous studies (23, 30), to examine the possible alteration of DC phenotypes in infected mice. We found that oral infection with *P. gingivalis* led to a significant increase of PD-L1 expression on DCs from CLNs, whereas the ΔKgp mutant and the commensal control failed to do so (**Fig. 2F–H**). Altogether, these results demonstrate for the first time that *P. gingivalis* promotes PD-L1 expression on DCs *in vitro* and *in vivo* in a manner that is dependent on the presence of the lysine-specific gingipain protease.

P. gingivalis infection enhances DC-PD-L1 expression through Akt and STAT3 signaling

P. gingivalis infection activates a multitude of signaling cascades that lead to inflammatory immune responses. Given that both Akt and STAT3 are critical drivers for the expression of PD-L1 (40, 41), we next examined if *P. gingivalis* infection-mediated upregulation of DC-PD-L1 was through Akt and STAT3. As expected, *P. gingivalis* infection robustly increased phosphorylation of Akt and STAT3 (**Fig. 3A** and **B**), but the ΔKgp mutant only slightly enhanced phosphorylation of STAT3 and failed to induce Akt phosphorylation (**Fig. 3C**). Given that the trend of Akt and STAT3 phosphorylation (**Fig. 3A–C**) was similar to that of PD-L1 expression (**Fig. 1G–J**) in response to the challenge of *P. gingivalis* and ΔKgp, it is possible that *P. gingivalis*–elevated PD-L1 is through the regulation of Akt and STAT3. To further prove this point, we utilized a specific Akt inhibitor, MK2206, to treat DCs and examine PD-L1 expression upon the challenge of *P. gingivalis*. We found that inhibition of Akt decreased PD-L1 expression on *P. gingivalis*–stimulated DCs in a dose-dependent manner (**Fig. 3D–F**) and was confirmed via Western blot (**Fig. 3G**). Moreover, Akt inhibition led to decreased phospho- and total-STAT3 (**Fig. 3G**), suggesting STAT3 might be a downstream target of Akt (**Fig. 3G**). This was inversely verified by the observation that STAT3 inhibition failed to affect Akt phosphorylation in *P. gingivalis*–stimulated DCs (**Fig. 3H**). Additionally, we found that chemical inhibition or gene silencing of STAT3, via siRNA, resulted in a significant decrease in PD-L1 expression in *P. gingivalis*–stimulated DCs (**Fig. 3I** and **J**). To exclude the possible off-target effects of the siRNA and verify the effect of STAT3 on PD-L1 expression, we transfected a plasmid encoding STAT3 into DCs and found that STAT3 overexpression (**Fig. 3K**) led to a significant increase of PD-L1 upon *P. gingivalis* challenge (**Fig. 3K** and **L**). These data suggest that the *P. gingivalis*–induced elevated PD-L1 expression on DCs was through modulation of Akt–STAT3 signaling.

P. gingivalis–mediated Akt–STAT3 signaling promotes PD-L1 expression and suppresses CD8⁺ T-cell activity

We next examined the possible influences of *P. gingivalis* on CD8⁺ T-cell activation. To do this, Flt3l-DCs were prepulsed with antigenic OVA peptide (SIINFEKL) at concentrations ranging from 0.1 to 10 ng/mL, followed by a challenge with *P. gingivalis* and coculture with OVA-specific, splenic CD8⁺ T cells from OT-I mice for 3 days. Because 1 ng/mL OVA stimulation was observed to produce the highest level of IL2 (Supplementary Fig. S2), we used this concentration throughout the following experiments. *P. gingivalis* treatment significantly elevated PD-L1 expression on DCs, which is consistent with our observations in **Fig. 1**, suggesting that *P. gingivalis* infection promotes the expression of PD-L1 in different contexts (**Fig. 4A**). Moreover, OVA-pulsed DCs effectively activated CD8⁺ T cells, represented by a significant increase of effector molecules, including Prf, GrB, and CD107a, and hallmark cytokines, IFNγ and IL2 (**Fig. 4B–G**). However, when antigen-pulsed DCs were challenged with *P. gingivalis*, the production of effector molecules and hallmark cytokines was significantly decreased (**Fig. 4B–G**), which was further confirmed by ELISA (**Fig. 4D** and **E**). These results suggest that *P. gingivalis* infection enhances PD-L1 expression and suppresses CD8⁺ T-cell activity.

To further determine whether *P. gingivalis*–mediated suppression of CD8⁺ T cells was through modulation of STAT3 and PD-L1, we first utilized a STAT3 inhibitor, WP-1066, to treat antigen-pulsed DCs, followed by challenge with *P. gingivalis* and coculture with CD8⁺ T cells. After 72 hours, we found that treatment with WP-1066 significantly reduced PD-L1 expression while concurrently elevating the expression of IFNγ, Prf, CD107a, and GrB from CD8⁺ T cells (**Fig. 5A–E**). Additionally, we also utilized a PD-L1 antagonist binding peptide, (D)-PPA, to block PD-L1/PD-1 binding to determine the role of PD-L1 in *P. gingivalis*–suppressed CD8⁺ T-cell activity. As expected, blockade of PD-L1 on DCs with (D)-PPA peptide significantly attenuated the suppressive effect of *P. gingivalis* infection on the

---

Figure 7.

P. gingivalis infection promotes PD-L1 expression on DCs and aggravates the progression of oral cancer in a syngeneic oral cancer model. **A,** A schematic model showing the experimental procedure. Eight- to 10-week-old C57B6/J mice (*n* = 5 to 7) were inoculated with MOC1 cells (1 × 10⁷; 0.2 mL) into the tongue [MOC1 cells were pretreated with or without *P. gingivalis* (MOI 10)], followed by repetitive challenge with *P. gingivalis*. **B,** Left: representative flow cytometry histograms showing the expression of PD-L1 on DCs from CLNs. Right: the percentage of CLN DCs expressing CD11b/CD11c/PD-L1. **C,** Left: representative pictures of tumors from mouse tongues from different groups; tumors depicted with a dotted line. Right: quantification of the average area of tumors in tongues. **D,** Representative H&E staining images of mouse tongues showing the largest diameter (red dotted line) of the tumor (scale bar, 5 mm and 200 μm as indicated). **E,** The alteration of the average of tumor's largest diameter was quantified to estimate the volume of tumors. **F** and **G,** The fluorescence intensity of positive staining cells with CD11c and PD-L1 in ROIs was quantified by the ImageJ after color deconvolution (minimum 5 ROI per slide and 3 consecutive slides every mouse, *n* > 5 mice per group). **F,** Quantification of the percentage of the CD11c/PD-L1–positive area showing the expression of CD11c and PD-L1 in *P. gingivalis*–treated mice. **G,** Representative immunofluorescence images showing the CD11c- and PD-L1–positive staining cells in *P. gingivalis*–treated mice (scale bar, 50 μm). **H–M,** The effect of ΔKgp mutant on DC-PD-L1 expression and tumor growth was examined using the same model as above (*n* = 5 mice). Additionally, the effect of established oral infection with *P. gingivalis* or ΔKgp followed by inoculation of uninfected MOC1 cells was analyzed using a modified procedure (**A;** shown with red fonts). The same methods were used to analyze DC-PD-L1 expression and tumor growth. **H–J,** Representative flow cytometry histograms (**H,** left), quantification of the percentage of positive cells (**H,** right), representative immunofluorescence images (scale bar, 50 μm; **I**), and quantification of the percentage of the CD11c/PD-L1–positive area (**J**) showing the expression of PD-L1 and/or CD11c on DCs from the CLNs or intratumoral cancer tissues of the mice that were orally preinfected with *P. gingivalis* or ΔKgp. **K–M,** Representative pictures of tumors from mouse tongues (**K**), quantification of the average area of tumors in tongues (**L**), quantification of the alteration of the tumor's largest diameter (**M**) were used to estimate the growth of tumors in *P. gingivalis* or ΔKgp preinfected mice. Each symbol represents an individual mouse, and data are shown as mean ± SE. Results are representative of two independent experiments. Statistical significance was determined by one-way ANOVA with the Tukey multiple comparisons test. *, *P* < 0.05; **, *P* < 0.01; ***, *P* < 0.001.

---

production of Prf, IL2, and GrB (**Fig. 5F–H**). Taken together, these data indicate *P. gingivalis* infection suppresses CD8$^+$ T-cell activity through STAT3-mediated PD-L1 expression on DC cells.

Infection of *P. gingivalis* dampens the cytotoxicity of CD8$^+$ T cells

To further assess the effect of *P. gingivalis* infection on the cytotoxicity of CD8$^+$ T cells, we next cocultured primed CD8$^+$ T cells with target cells (EL4 cell line) that were prestained with two different concentrations of CFSE (1 and 0.1 μmol/L; see Materials and Methods). By gating CFSE$^+$CD8$^-$ cells, we excluded the possible interference of the dead cells in further analysis (**Fig. 6A**). *P. gingivalis* significantly reduced CD8$^+$ T-cell cytotoxicity in all groups (three different effector/target ratios), represented by the amount of lysed target cells (**Fig. 6B** and **C**). The percentage of lysed target cells in the groups primed by *P. gingivalis* pretreated DCs was significantly lower than those of non–*P. gingivalis* treated cells (**Fig. 6C**). Moreover, STAT3 inhibition significantly elevated CD8$^+$ T-cell cytotoxicity upon the challenge of *P. gingivalis* (**Fig. 6D**). Notably, infection with ΔKgp mutant significantly increased lysed target cells compared with the wild-type parent strain (**Fig. 6E**). Altogether, these results demonstrate that *P. gingivalis* infection impairs the cytotoxicity of CD8$^+$ T cells through modulation of STAT3 activation and PD-L1 expression in DCs, and this ability is dependent, at least partially, on the presence of the lysine-specific gingipain protease.

P. gingivalis infection promotes PD-L1 expression on DCs and aggravates progression of oral cancer in a syngeneic oral cancer model

To assess the effects of *P. gingivalis* infection on DC-PD-L1 expression and CD8$^+$ T-cell activity in oral cancer, we next utilized a syngeneic mouse model in which MOC1 cells pretreated with or without *P. gingivalis* were inoculated into mouse tongues (**Fig. 7A**). We found that CD11c$^+$MHC-II$^+$ DCs from the lymph nodes of *P. gingivalis*–infected mice had a significantly higher expression of PD-L1 than DCs from control mice (**Fig. 7B**; $P < 0.001$). However, treatment with a STAT3 inhibitor or feeding with antibiotic water significantly decreased PD-L1 expression (**Fig. 7B**). In addition, *P. gingivalis* infection led to a significant increase of PD-1 expression on CD8$^+$ T cells (Supplementary Fig. S2), suggesting both PD-L1 and PD-1 could be the target of *P. gingivalis* to modulate CD8$^+$ T-cell activity. Overexpression of PD-L1 on DCs has been demonstrated to reduce the efficacy of immunotherapy and aggravate cancer progression (13, 14). We therefore examined if *P. gingivalis* infection would aggravate the progression of oral cancer. MOC1 cells pretreated with *P. gingivalis* developed into larger tumors than that of untreated MOC1 cells, estimated by the area of the tumor mass in tongue tissues as described in a previous study (**Fig. 7C**; see Materials and Methods; ref. 31). However, mice infected with *P. gingivalis* followed by treatment with antibiotics or WP-1066 had a significant decrease in tumor mass compared with the mice infected with *P. gingivalis* only or the sham control groups (**Fig. 7C**). These results are consistent with a multitude of previous studies showing *P. gingivalis* infection promotes tumor growth and worsens the prognosis of cancer patients (18–20, 22, 42). Given there is not a widely accepted measuring approach to estimate the tumor volume in a MOC1-mediated syngeneic model, we utilized the clinical RECIST 1.1 guidelines (18, 32) and estimated the tumor volume using the longest dimension of the tumor mass. As expected, by measuring the largest diameter of tumor mass from H&E-stained images (**Fig. 7D** and **E**), we observed a similar trend in tumor volume alteration in various groups, as was observed by

measuring the area of tumor mass (**Fig. 7D** and **E**). In addition, we also examined expression of PD-L1 by DCs that infiltrated tumor tissues using immunofluorescence. *P. gingivalis* infection significantly promoted expression of PD-L1 on intratumoral DCs, but antibiotic or STAT3 inhibition significantly decreased it (**Fig. 7F** and **G**, $P < 0.001$), which is consistent with the alteration of PD-L1 expression on DCs from lymph nodes.

To examine the clinical relevance of *P. gingivalis* infection to tumor progression under the natural infection milieu of the oral cavity, we orally infected mice with *P. gingivalis* first and then inoculated uninfected MOC1 cells into mouse tongues. The expression of PD-L1 on DCs from CLNs and tumor tissues and the growth of tumors were examined as described above. We found that DC-PD-L1 expression from the mice orally preinfected with *P. gingivalis* was significantly higher than that of uninfected controls, despite being slightly lower than the mice inoculated with preinfected MOC1 cells and subsequent oral infection with *P. gingivalis* (**Fig. 7H–J**, $P < 0.001$). Moreover, the trends of tumor volume alteration were similar to those of DC-PD-L1 expression (**Fig. 7K–M**, $P < 0.001$), indicating that *P. gingivalis* infection may be involved in tumor progression via alteration of the immune landscape in the tumor microenvironment. In addition, infection with *P. gingivalis* ΔKgp mutant in MOC1 cells failed to significantly promote PD-L1 expression and tumor progression (**Fig. 7H–M**, $P < 0.001$). Altogether, these data validated our *in vitro* results and demonstrated that *P. gingivalis* infection enhances PD-L1 expression and exacerbates the progression of oral cancer in a syngeneic mouse model.

Discussion

P. gingivalis infection has been shown to promote cancer progression by the modification of cell cycle, proliferation, apoptosis, and tumor cell responses to chemotherapeutic drugs (18, 20, 43, 44). Ours and other recent studies demonstrate that *P. gingivalis* infection facilitates macrophage polarization toward M2 in the inflammatory milieu of oral cavity, thereby exacerbating the prognosis of cancer patients (22, 23). In this study, we found for the first time that *P. gingivalis* infection promotes expression of DC-PD-L1 and suppresses the cytotoxicity of CD8$^+$ T cells, which could be another immune mechanism *P. gingivalis* uses to aggravate cancer progression. Moreover, we showed that *P. gingivalis* infection promotes the expression of PD-1 on CD8$^+$ T cells from mouse CLNs, suggesting both PD-L1 and its receptor could be manipulated by *P. gingivalis* to evade immune attack and suppress the host immune responses against tumors. Therefore, our findings provide insights to the immunosuppressive property of *P. gingivalis* and aids in identifying potential interventional targets to improve the effectiveness of immunotherapies in the future.

The regulation of PD-L1 expression is a complex and highly coordinated series of signaling events. It occurs through dynamic modulation of multiple transcriptional factors (TF) such as STAT3, HIF, Myc, AP-1, and NF-κB or autocrine signaling (39). Although we found that *P. gingivalis*–activated Akt–STAT3 was critical for DC-PD-L1 expression, we cannot exclude the possible regulatory function of other TFs or the involvement of autocrine signaling pathways in this process. One possible autocrine signaling pathway is *P. gingivalis*–mediated secretion of interferon, which was demonstrated as a dominant inducer of PD-L1 (14). Whereas recent studies report opposite effects of *P. gingivalis* infection on the production interferon and its signaling (45, 46), our results clearly showed that neutralization of either type I IFN receptor or type II

interferon did not affect *P. gingivalis*–induced elevation of PD-L1 expression on DCs, suggesting interferon signaling may not be involved in this process.

In this study, we did not observe a substantial change of PD-L1 in *S. sanguinis*–stimulated DCs, but we cannot exclude the possibility that this bacterium may affect PD-L1 expression by altering the growth of *P. gingivalis* and/or the composition of the local microbiome in the infectious milieu. Previous studies have reported that commensal bacteria and composition of the microbiome indeed affect the efficiency of anti–PD-L1 immunotherapy (47, 48). Considering the *de facto* status of the microbiome in the oral cancer microenvironment, the indirect impact of other oral microbes on PD-L1 expression warrants further investigation to characterize the influences of *P. gingivalis* and other bacteria, both individually and in combination, on the response of cancer patients to PD-1/PD-L1 blockade immunotherapy.

Recent studies have demonstrated that PD-L1 can bind B7.1 (CD80) *in cis* on DCs and prevent PD-L1 binding to PD-1 on T cells (42, 49). Therefore, *P. gingivalis*–elevated PD-L1 on DCs may mediate inhibitory effects on CD8$^+$ T-cell activity by a two-pronged strategy: (i) strengthening PD-L1/PD-1 interaction *in trans* between DCs and T cells, thus enhancing PD-1–mediated inhibitory signaling on T cells and (ii) intensifying the PD-L1/B7.1 interaction *in cis* on DCs, leading to increased sequestration of B7.1 that would reduce the costimulatory signals of B7.1/CD28 and lead to T-cell immune suppression. On the other hand, because B7.1 also competitively binds CTLA-4, we cannot exclude the possibility that sequestered B7.1 by increased PD-L1 might also repress CTLA-4–mediated suppressive signals, offsetting the effect of *P. gingivalis* on CD8$^+$ T-cell cytotoxicity to some degree. Additionally, despite that PD-L1:B7.1 *cis*-heterodimerization inhibits both PD-L1:PD-1 and B7.1:CTLA-4 interactions, it was reported to preserve the ability of CD80 to activate the T-cell costimulatory molecule CD28 (50). Expression of PD-L1 on antigen-presenting cells robustly reduces CTLA-4–mediated *trans*-endocytosis of CD80 (50). These results indicate that an increase of PD-L1 may lead to several negative feedback loops to restrain the immunosuppressive effect that PD-L1 exerts on CD8$^+$ T cells. Therefore, further studies focusing on the comprehensive impact of *P. gingivalis* infection on PD-1, B7.1, and CTLA4 will advance our understanding of this complex network and provide more innovative insights into the strategies *P. gingivalis* exploits to manipulate tumor immune responses.

To the best of our knowledge, we have demonstrated for the first time that *P. gingivalis* suppresses CD8$^+$ T-cell cytotoxicity through promoting the expression of DC-PD-L1. It is well known that the decrease of IFNγ, Prf, GrB, and CD107a will directly reduce the granule exocytosis of CD8$^+$ T cells and reduce their capability to eliminate infected cells, which may aggravate some virus infection–mediated chronic inflammatory diseases. Some studies have reported this, showing *P. gingivalis* infection exacerbates the infection of Epstein–Barr virus (EBV), human immunodeficiency virus, and hepatitis B virus (HBV)/hepatitis C virus, and thus aggravates related diseases (46). Although various distinct mechanisms are reported in different contexts, *P. gingivalis* enhances PD-L1 expression and debilitated cytotoxic T cells could compromise the "antiviral state" of immune cells and aggravate infection with viruses in general, potentially including SARS-CoV2. Therefore, future investigations on the interactions between *P. gingivalis* and viruses will yield insights into the pathogenicity of *P. gingivalis*, aiding in the development of novel strategies to optimize the efficacy of immunotherapies for the control of virus infection.

Oral administration of metronidazole to mice bearing *P. gingivalis*–exposed MOC1 cells resulted in a significant decrease in tumor growth compared with mice treated with the vehicle alone. Treatment with metronidazole was associated with a significant decrease in tumor volume and PD-L1 expression on DCs from both CLNs and tumoral tissues. These results indicate the potential for control of *P. gingivalis* infection as a target for oral cancer therapy. However, it may be premature to advocate the use of metronidazole. Because metronidazole targets a group of anaerobic bacteria including some anaerobes with established interactions with *P. gingivalis*, the development of a *P. gingivalis*–specific antimicrobial agent may be required. Additionally, further studies on the effect of metronidazole on cancer cell immune evasion and related clinical evidence are required to comprehensively assess the influence of antibiotics on the progression and prognosis of oral cancer.

In summary, we have demonstrated for the first time that *P. gingivalis* infection elevates PD-L1 expression on the surface of DCs, suppresses cytotoxicity of CD8$^+$ T cells, and aggravates the progression of oral cancer. Moreover, we revealed that the presence of gingipains and *P. gingivalis*–mediated activation of Akt–STAT3 signaling are critical for the upregulation of DC-PD-L1 and subsequent suppression of CD8$^+$ T-cell cytotoxicity. Considering the successful application of antibodies targeting PD-1 and its ligands in cancer immunotherapy, our findings provide more insights into immunesuppressive properties of *P. gingivalis* and identify potential targets to manipulate the immune response and thereby improve the efficacy of cancer immunotherapies.

Authors' Disclosures

Authors' Contributions

J. Ren: Data curation, formal analysis, investigation, visualization, methodology, writing–original draft. **X. Han:** Data curation, software, formal analysis, validation, investigation, visualization, methodology. **H. Lohner:** Formal analysis, investigation, methodology, writing–review and editing. **R.G. Hoyle:** Data curation, investigation, writing–review and editing. **J. Li:** Resources, data curation, supervision, investigation. **S. Liang:** Conceptualization, data curation, formal analysis, supervision, methodology. **H. Wang:** Conceptualization, resources, formal analysis, supervision, funding acquisition, validation, investigation, methodology, writing–original draft, project administration, writing–review and editing.

Acknowledgments

Note

References

1. Pamer E, Cresswell P. Mechanisms of MHC class I–restricted antigen processing. Annu Rev Immunol 1998;16:323–58.
2. Wong P, Pamer EG. CD8 T cell responses to infectious pathogens. Annu Rev Immunol 2003;21:29–70.
3. Ribas A, Wolchok JD. Cancer immunotherapy using checkpoint blockade. Science 2018;359:1350–5.
4. Wykes MN, Lewin SR. Immune checkpoint blockade in infectious diseases. Nat Rev Immunol 2018;18:91–104.
5. Ohaegbulam KC, Assal A, Lazar-Molnar E, Yao Y, Zang X. Human cancer immunotherapy with antibodies to the PD-1 and PD-L1 pathway. Trends Mol Med 2015;21:24–33.
6. Bocanegra A, Fernandez-Hinojal G, Zuazo-Ibarra M, Arasanz H, Garcia-Granda MJ, Hernandez C, et al. PD-L1 expression in systemic immune cell populations as a potential predictive biomarker of responses to PD-L1/PD-1 blockade therapy in lung cancer. Int J Mol Sci 2019;20:1631.
7. Lu C, Redd PS, Lee JR, Savage N, Liu K. The expression profiles and regulation of PD-L1 in tumor-induced myeloid-derived suppressor cells. Oncoimmunology 2016;5:e1247135.
8. Garber K. Predictive biomarkers for checkpoints, first tests approved. Nat Biotechnol 2015;33:1217–8.
9. Powles T, Eder JP, Fine GD, Braiteh FS, Loriot Y, Cruz C, et al. MPDL3280A (anti-PD-L1) treatment leads to clinical activity in metastatic bladder cancer. Nature 2014;515:558–62.
10. Sabatier R, Finetti P, Mamessier E, Adelaide J, Chaffanet M, Ali HR, et al. Prognostic and predictive value of PDL1 expression in breast cancer. Oncotarget 2015;6:5449–64.
11. Sunshine J, Taube JM. PD-1/PD-L1 inhibitors. Curr Opin Pharmacol 2015;23:32–8.
12. Rashidian M, LaFleur MW, Verschoor VL, Dongre A, Zhang Y, Nguyen TH, et al. Immuno-PET identifies the myeloid compartment as a key contributor to the outcome of the antitumor response under PD-1 blockade. Proc Natl Acad Sci U S A 2019;116:16971–80.
13. Oh SA, Wu DC, Cheung J, Navarro A, Xiong H, Cubas R, et al. PD-L1 expression by dendritic cells is a key regulatory of T-cell immunity in cancer. Nature Cancer 2020;1:681–91.
14. Peng Q, Qiu X, Zhang Z, Zhang S, Zhang Y, Liang Y, et al. PD-L1 on dendritic cells attenuates T cell activation and regulates response to immune checkpoint blockade. Nat Commun 2020;11:4835.
15. Kim HR, Ha SJ, Hong MH, Heo SJ, Koh YW, Choi EC, et al. PD-L1 expression on immune cells, but not on tumor cells, is a favorable prognostic factor for head and neck cancer patients. Sci Rep 2016;6:36956.
16. Herbst RS, Soria JC, Kowanetz M, Fine GD, Hamid O, Gordon MS, et al. Predictive correlates of response to the anti-PD-L1 antibody MPDL3280A in cancer patients. Nature 2014;515:563–7.
17. Olsen I, Yilmaz O. Modulation of inflammasome activity by porphyromonas gingivalis in periodontitis and associated systemic diseases. J Oral Microbiol 2016;8:30385.
18. Gao S, Liu Y, Duan X, Liu K, Mohammed M, Gu Z, et al. Porphyromonas gingivalis infection exacerbates oesophageal cancer and promotes resistance to neoadjuvant chemotherapy. Br J Cancer 2021;125:433–44.
19. Wang X, Jia Y, Wen L, Mu W, Wu X, Liu T, et al. Porphyromonas gingivalis promotes colorectal carcinoma by activating the hematopoietic NLRP3 inflammasome. Cancer Res 2021;81:2745–59.
20. Gao S, Li S, Ma Z, Liang S, Shan T, Zhang M, et al. Presence of porphyromonas gingivalis in esophagus and its association with the clinicopathological characteristics and survival in patients with esophageal cancer. Infect Agent Cancer 2016;11:3.
21. Wen L, Mu W, Lu H, Wang X, Fang J, Jia Y, et al. Porphyromonas gingivalis promotes oral squamous cell carcinoma progression in an immune microenvironment. J Dent Res 2020;99:666–75.
22. Liu S, Zhou X, Peng X, Li M, Ren B, Cheng G, et al. Porphyromonas gingivalis promotes immunoevasion of oral cancer by protecting cancer from macrophage attack. J Immunol 2020;205:282–9.
23. Ren J, Han X, Lohner H, Liang R, Liang S, Wang H. Serum- and glucocorticoid-inducible kinase 1 promotes alternative macrophage polarization and restrains inflammation through FoxO1 and STAT3 signaling. J Immunol 2021;207:268–80.
24. Groeger S, Denter F, Lochnit G, Schmitz ML, Meyle J. Porphyromonas gingivalis cell wall components induce programmed death ligand 1 (PD-L1) expression on human oral carcinoma cells by a receptor-interacting protein kinase 2 (RIP2)-dependent mechanism. Infect Immun 2020;88:e00051–20.
25. Gemmell E, Drysdale KE, Seymour GJ. Gene expression in splenic CD4 and CD8 cells from BALB/c mice immunized with Porphyromonas gingivalis. J Periodontol 2006;77:622–33.
26. Moutsopoulos NM, Kling HM, Angelov N, Jin W, Palmer RJ, Nares S, et al. Porphyromonas gingivalis promotes Th17 inducing pathways in chronic periodontitis. J Autoimmun 2012;39:294–303.
27. Inaba K, Inaba M, Romani N, Aya H, Deguchi M, Ikehara S, et al. Generation of large numbers of dendritic cells from mouse bone marrow cultures supplemented with granulocyte/macrophage colony-stimulating factor. J Exp Med 1992;176:1693–702.
28. Brasel K, De Smedt T, Smith JL, Maliszewski CR. Generation of murine dendritic cells from flt3-ligand-supplemented bone marrow cultures. Blood 2000;96:3029–39.
29. Bustos-Moran E, Blas-Rus N, Alcaraz-Serna A, Iborra S, Gonzalez-Martinez J, Malumbres M, et al. Aurora a controls CD8(+) T cell cytotoxic activity and antiviral response. Sci Rep 2019;9:2211.
30. Han X, Ren J, Lohner H, Yakoumatos L, Liang R, Wang H. SGK1 negatively regulates inflammatory immune responses and protects against alveolar bone loss through modulation of TRAF3 activity. J Biol Chem 2022;298:102036.
31. Czerninski R, Amornphimoltham P, Patel V, Molinolo AA, Gutkind JS. Targeting mammalian target of rapamycin by rapamycin prevents tumor progression in an oral-specific chemical carcinogenesis model. Cancer Prev Res (Phila) 2009;2:27–36.
32. Schwartz LH, Litiere S, de Vries E, Ford R, Gwyther S, Mandrekar S, et al. RECIST 1.1-update and clarification: from the RECIST committee. Eur J Cancer 2016;62:132–7.
33. Crowe AR, Yue W. Semi-quantitative determination of protein expression using immunohistochemistry staining and analysis: an integrated protocol. Bio Protoc 2019;9:e3465.
34. Sumpter TL, Thomson AW. The STATus of PD-L1 (B7-H1) on tolerogenic APCs. Eur J Immunol 2011;41:286–90.
35. Parajuli P, Mosley RL, Pisarev V, Chavez J, Ulrich A, Varney M, et al. Flt3 ligand and granulocyte-macrophage colony-stimulating factor preferentially expand and stimulate different dendritic and T-cell subsets. Exp Hematol 2001;29:1185–93.
36. Lanzavecchia A, Sallusto F. Dynamics of T lymphocyte responses: intermediates, effectors, and memory cells. Science 2000;290:92–7.
37. Moser M, Murphy KM. Dendritic cell regulation of TH1-TH2 development. Nat Immunol 2000;1:199–205.
38. Pistillo MP, Carosio R, Banelli B, Morabito A, Mastracci L, Ferro P, et al. IFN-gamma upregulates membranous and soluble PD-L1 in mesothelioma cells: potential implications for the clinical response to PD-1/PD-L1 blockade. Cell Mol Immunol 2020;17:410–1.
39. Sun C, Mezzadra R, Schumacher TN. Regulation and function of the PD-L1 checkpoint. Immunity 2018;48:434–52.
40. Song TL, Nairismagi ML, Laurensia Y, Lim JQ, Tan J, Li ZM, et al. Oncogenic activation of the STAT3 pathway drives PD-L1 expression in natural killer/T-cell lymphoma. Blood 2018;132:1146–58.
41. Lastwika KJ, Wilson W 3rd, Li QK, Norris J, Xu H, Ghazarian SR, et al. Control of PD-L1 expression by oncogenic activation of the AKT-mTOR pathway in non-small cell lung cancer. Cancer Res 2016;76:227–38.
42. Chaudhri A, Xiao Y, Klee AN, Wang X, Zhu B, Freeman GJ. PD-L1 binds to B7–1 only in cis on the same cell surface. Cancer Immunol Res 2018;6:921–9.
43. Lamont RJ, Fitzsimonds ZR, Wang H, Gao S. Role of porphyromonas gingivalis in oral and orodigestive squamous cell carcinoma. Periodontol 2000 2022;89:154–65.
44. Ohshima J, Wang Q, Fitzsimonds ZR, Miller DP, Sztukowska MN, Jung YJ, et al. Streptococcus gordonii programs epithelial cells to resist ZEB2 induction by porphyromonas gingivalis. Proc Natl Acad Sci U S A 2019;116:8544–53.
45. Mizraji G, Nassar M, Segev H, Sharawi H, Eli-Berchoer L, Capucha T, et al. Porphyromonas gingivalis promotes unrestrained type i interferon production by dysregulating TAM signaling via MYD88 degradation. Cell Rep 2017;18:419–31.
46. Rodriguez-Hernandez CJ, Sokoloski KJ, Stocke KS, Dukka H, Jin S, Metzler MA, et al. Microbiome-mediated incapacitation of interferon lambda production in the oral mucosa. Proc Natl Acad Sci U S A 2021;118:e2105170118.

47. Matson V, Fessler J, Bao R, Chongsuwat T, Zha Y, Alegre ML, et al. The commensal microbiome is associated with anti-PD-1 efficacy in metastatic melanoma patients. Science 2018;359:104–8.

48. Derosa L, Routy B, Kroemer G, Zitvogel L. The intestinal microbiota determines the clinical efficacy of immune checkpoint blockers targeting PD-1/PD-L1. Oncoimmunology 2018;7:e1434468.

49. Zhao Y, Harrison DL, Song Y, Ji J, Huang J, Hui E. Antigen-presenting cell-intrinsic PD-1 neutralizes PD-L1 in cis to Attenuate PD-1 signaling in T cells. Cell Rep 2018;24:379–90.

50. Zhao Y, Lee CK, Lin CH, Gassen RB, Xu X, Huang Z, et al. PD-L1:CD80 Cis-heterodimer triggers the Co-stimulatory receptor CD28 while repressing the inhibitory PD-1 and CTLA-4 pathways. Immunity 2019;51:1059–73.